

Scattering of 41-MeV α particles and 46-MeV ${}^3\text{He}$ from ${}^{27}\text{Al}$, ${}^{28}\text{Si}$, ${}^{29}\text{Si}$, and ${}^{30}\text{Si}$

C. B. Fulmer

Oak Ridge National Laboratory* Oak Ridge, Tennessee 37830

G. Mariolopoulos, G. Bagieu, A. J. Cole, R. de Swiniarski, and D. H. Koang

Institute des Sciences Nucléaires (IN2P3 et U.S.M.G.), 38044 Grenoble Cedex, France

(Received 15 November 1977)

Elastic scattering angular distributions were measured for 46-MeV ${}^3\text{He}$ over the $\sim 30^\circ$ – 110° range and for 41-MeV α particles over the $\sim 25^\circ$ – 150° range for the neighboring targets ${}^{27}\text{Al}$, ${}^{28,29,30}\text{Si}$. For α particles, $l = 2$ inelastic scattering data were also obtained at angles beyond $\sim 50^\circ$. For ${}^3\text{He}$ the three Si targets yield similar angular distributions that are different from that of ${}^{27}\text{Al}$ at angles larger than $\sim 55^\circ$. The elastic α -particle data supplement earlier back angle data to yield almost complete angular distributions. The ${}^{28}\text{Si}$ α -particle elastic angular distribution exhibits an anomaly in the 80° – 150° region. The ${}^3\text{He}$ data were fitted by optical model potentials with either volume or surface absorption. To fit all of the α -particle elastic scattering data, potentials with both volume and surface absorption, with separate geometry parameters, were needed. Distorted-wave Born-approximation analyses of the α -particle inelastic scattering data yield values of β_2 that are in reasonable agreement with values obtained from analyses of scattering at other energies and incident particles.

NUCLEAR REACTIONS (${}^3\text{He}$, ${}^3\text{He}$) at MeV and (α , α') at 41 MeV from, ${}^{27}\text{Al}$, ${}^{28,29,30}\text{Si}$; enriched targets. Measured $\sigma(\theta)$; performed optical model and DWBA analyses; deduced scattering potentials and β_2 values.

I. INTRODUCTION

At energies of a few tens of MeV both α and ${}^3\text{He}$ elastic scattering angular distributions exhibit pronounced structure which usually varies smoothly with target mass and incident particle energy. The elastic scattering has been generally well described by the optical model in that the parameters of the potential have been found to vary smoothly with target mass (A) and bombarding energy (E_{lab}). There are cases, however, of low energy α scattering from light targets which show irregular variations with A and/or E_{lab} which may be due to compound nucleus or nuclear structure effects. This is particularly true for targets in the s - d shell.

There are also cases where significant differences are observed between the scattering from heavier neighboring even and odd targets. For example, at angles beyond $\sim 50^\circ$, the elastic angular distributions of both ${}^3\text{He}$ and α particles for ${}^{59}\text{Co}$ ($I = \frac{7}{2}$) have minima that are much shallower than for ${}^{60}\text{Ni}$ ($I = 0$).^{1,2}

In optical model analyses¹ of ${}^3\text{He}$ elastic scattering from a number of neighboring target pairs, the target spin effects were found to be consistent with a real spin-orbit well depth ~ 1 MeV deeper for the $I \neq 0$ targets than for the $I = 0$ targets. For α -particle scattering, a theoretical study by Rawitscher³ has shown the target spin-orbit term

to be much smaller in the α -nucleus optical model potential.

Target spin differences for ${}^3\text{He}$ scattering have also been accounted for by a quadrupole contribution to the elastic scattering from the $I \neq 0$ nucleus⁴; for the case of ${}^{59}\text{Co}$ and ${}^{60}\text{Ni}$, the target spin effect for both ${}^3\text{He}$ and α -particle scattering has been accounted for by the quadrupole contribution.⁵ For an $I = \frac{1}{2}$ target nucleus the quadrupole contribution to the elastic scattering is zero; thus data from neighboring targets that include an $I = \frac{1}{2}$ nucleus are favorable cases for further study to determine whether there are target spin effects that cannot be attributed to such a contribution.

In the work reported here, α -particle and ${}^3\text{He}$ elastic scattering angular distributions were measured for targets of ${}^{27}\text{Al}$ ($I = \frac{5}{2}$), ${}^{28,30}\text{Si}$ ($I = 0$), and ${}^{29}\text{Si}$ ($I = \frac{1}{2}$). An incident beam energy of ~ 40 MeV was selected for the α -particle scattering because measurements on these targets at this energy^{6,7} had been obtained for the angular region near 180° . For the ${}^3\text{He}$ scattering, an incident particle energy of 46 MeV was selected. Earlier measurements around 30 MeV (Ref. 8) had shown only a hint of target spin effects, while 60 MeV ${}^3\text{He}$ elastic scattering from ${}^{27}\text{Al}$ shows very little structure in the angular distribution beyond $\sim 60^\circ$.⁹

After a brief description of the experiment in Sec. II, the experimental results are presented in Sec. III. Optical model analyses of elastic data

from the four target nuclei are described in Sec. IV, and Sec. V presents a comparison of distorted-wave Born-approximation (DWBA) calculations with our inelastic scattering data. A short summary and discussion are presented in Sec. VI.

II. EXPERIMENT

The data were obtained with beams of α and ${}^3\text{He}$ particles from the Grenoble cyclotron. Beam intensities as high as 150 nA on target were used.

For the α -particle measurements, four silicon surface barrier detectors were mounted on two movable arms in the scattering chamber. For the ${}^3\text{He}$ measurements, particle identification was required and was achieved by using telescopes of ΔE and E detectors of 300 and 2500- μm thickness, respectively. Four such telescopes were used. All detectors were cooled to $\sim -20^\circ\text{C}$ by thermoelectric devices. Angular acceptance of the detectors was $\sim 0.6^\circ$.

The silicon isotope targets were in the form of silicon oxide evaporated onto plastic backing. The oxygen and carbon impurities limited measurements of elastic scattering to angles beyond $\sim 24^\circ$ and inelastic measurements to angles beyond $\sim 45^\circ$. Enrichments of the principal isotopes were 99.8%, 95.3%, and 95.6%, respectively, for the ${}^{28}\text{Si}$, ${}^{29}\text{Si}$, and ${}^{30}\text{Si}$ targets. Target thicknesses of silicon as determined by measuring elastic scattering of 9-MeV protons were 139, 162, and 120 $\mu\text{g}/\text{cm}^2$, respectively, for ${}^{28}\text{Si}$, ${}^{29}\text{Si}$, and ${}^{30}\text{Si}$. The aluminum target was a self supporting foil 950 $\mu\text{g}/\text{cm}^2$ as determined by α -particle energy loss in the foil.

III. EXPERIMENTAL RESULTS

A. α -particle scattering

The α -particle elastic scattering cross sections are presented in Fig. 1 (along with the ${}^3\text{He}$ elastic scattering data) where they are plotted as ratio to Rutherford scattering cross sections.⁶ Data near 180° , obtained earlier at near the same energy,⁷ are included in the α -particle angular distributions shown in Fig. 1.

It is observed that the elastic α -particle angular distributions may be divided into three distinctive regions—forward of $\sim 80^\circ$, $\sim 80^\circ$ – 150° , and back of $\sim 150^\circ$. In the forward region, data from the four targets exhibit very similar diffraction patterns. We note that for ${}^{27}\text{Al}$, ${}^{28}\text{Si}$, and ${}^{29}\text{Si}$, values of σ/σ_R are about equal at each of the three most forward maxima, which suggests that the absolute normalizations do not contain large errors. For ${}^{30}\text{Si}$, the second and third maxima could imply that the absolute normalization may be 10–20% low.

The second angular region is more interesting in

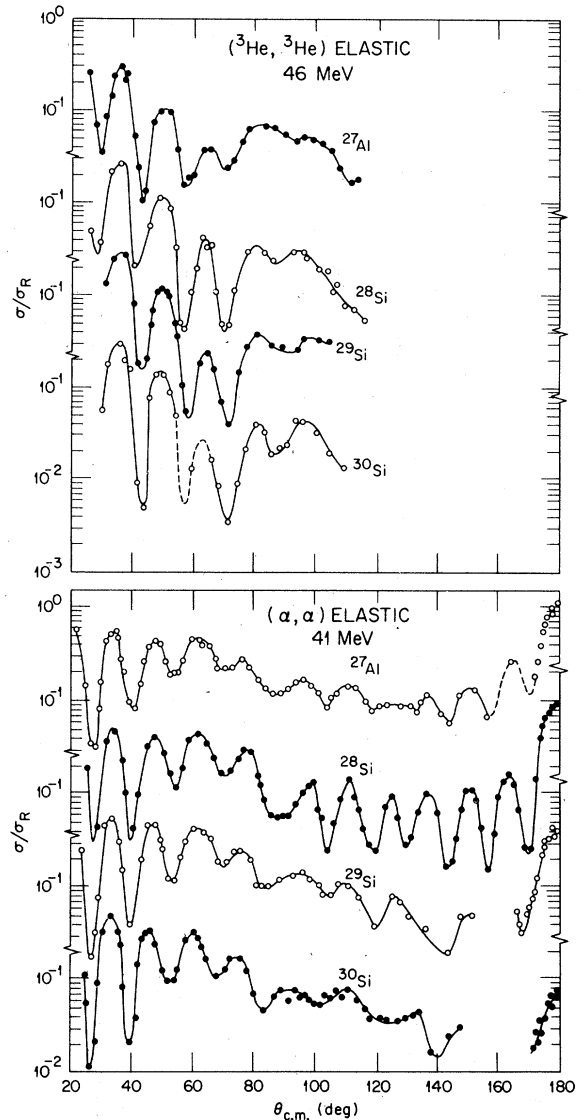


FIG. 1. Elastic scattering angular distributions plotted as ratio-to-Rutherford scattering cross sections. The α -particle data back of 150° are from Ref. 7. The curves are drawn to guide the eye.

that pronounced differences between the targets occur. The ${}^{27}\text{Al}$ and ${}^{29}\text{Si}$ data in this region are similar, and both are different from that of ${}^{28}\text{Si}$. Furthermore, the ${}^{28}\text{Si}$ angular distribution is very different from that of ${}^{30}\text{Si}$; both are $I=0$ nuclei, so the observed difference in this angular region cannot be attributed to target spin effects. We note that the present 41-MeV α -particle elastic scattering angular distribution for ${}^{28}\text{Si}$ is very similar to one measured at 39.5 MeV in earlier work.¹⁰

Quadrupole coupling contributions are largest at the elastic scattering minima, both in absolute

and relative magnitude. For ^{27}Al , the cross sections in the minima near 40° , 55° , and 70° are larger than for the three Si targets and provide some indication of a quadrupole contribution to the elastic scattering from ^{27}Al . The differences observed in this angular region are comparable to those in the 42-MeV α -particle scattering data from $^{24,25,26}\text{Mg}$ reported by Blair and Naquib.¹¹ The latter data, however, extend only to $\sim 70^\circ$ and do not indicate whether the distinctive behavior at larger angles observed in the present ^{28}Si data also characterize the ^{24}Mg elastic scattering.

Other examples of α -particle scattering from ^{27}Al and ^{28}Si include data at 22 MeV reported by Lega and Marq¹² and at 27.5 MeV reported by Bobrowska *et al.*¹³ While these lower energy data extend to almost 180° , the unusual behavior in the present 41-MeV data for ^{28}Si at angles beyond $\sim 70^\circ$ is not observed in the 22 and 27.5-MeV data.

Pronounced differences in the 41-MeV α -particle scattering from the four targets are also observed in the region beyond 150° . The angular distributions from ^{27}Al and ^{28}Si exhibit a strong back angle rise which is attenuated for ^{29}Si and attenuated further for ^{30}Si . It has been suggested that the magnitude of the maximum at 180° may be related to the neutron number of the target.¹⁴

B. ^3He scattering

The measured angular distributions for ^3He elastic scattering are also presented in Fig. 1. At angles forward of $\sim 55^\circ$ the four angular distributions are similar. At larger angles, data from the three silicon targets are similar but different from that of ^{27}Al . The differences are qualitatively like those observed earlier¹ for ^{59}Co and ^{60}Ni but are larger in relative magnitudes. The similarity of the elastic angular distributions for the three Si targets (which include the $I = \frac{1}{2}$ isotope ^{29}Si) suggests that for ^3He scattering, target spin effects could be principally due to quadrupole contributions.

A careful examination, however, raises a question of whether the differences are indeed due to quadrupole coupling. In Ref. 5 the quadrupole contribution was deduced from the measured quadrupole moment of the odd nucleus ground state and the measured $B(E2)$ for excitation of the corresponding 2^+ state in the even nucleus. For the case of ^{59}Co and ^{60}Ni this yielded

$$\sigma_{e1}(^{59}\text{Co}) \approx \sigma_{e1}(^{60}\text{Ni}) + 0.2\sigma_{\text{inel}}(^{60}\text{Ni}, 0^+ \rightarrow 2^+).$$

In the present case, by using a quadrupole moment for ^{27}Al of 15 fm^2 (Ref. 15) and a $B(E2)$ for ^{28}Si of $315 e^2 \text{ fm}^4$ (Ref. 16) one obtains the result

$$\sigma_{e1}(^{27}\text{Al}) \approx \sigma_{e1}(^{28}\text{Si}) + 0.038\sigma_{\text{inel}}(^{28}\text{Si}, 0^+ \rightarrow 2^+).$$

This implies that in the region of the deep minimum (at 70° in the ^{28}Si elastic angular distribution) the inelastic scattering to the lowest 2^+ level must be larger than the elastic scattering by a factor of ~ 100 to fully account for the difference by a quadrupole contribution to ^{27}Al elastic scattering. Unfortunately, ^3He inelastic cross sections were not obtained, but an upper limit of 15 for the ratio σ_{2^+}/σ_{e1} could be inferred from the pulse height spectra. It thus appears that the observed differences in 46-MeV ^3He scattering from ^{27}Al and ^{28}Si are not principally due to quadrupole contributions.

C. Inelastic scattering

Background due to target backing limited α -particle inelastic scattering measurements for the silicon targets to angles larger than $\sim 50^\circ$ and prevented any usable ^3He inelastic scattering measurements.

Inelastic scattering angular distributions for α particles were obtained for the lowest 2^+ states in $^{28,30}\text{Si}$ and the $\frac{3}{2}^+$ level at 1.28 MeV in ^{29}Si . For ^{27}Al more complete angular distributions were obtained for the two strongest peaks in the energy spectra. These are the $\frac{7}{2}^+$ level at 2.21 MeV and the unresolved doublet $\frac{3}{2}^+$ at 2.98 MeV and $\frac{9}{2}^+$ at 3.00 MeV; the latter is believed to be principally due to excitation of the $\frac{9}{2}^+$ level. These are the two highest spin levels of the multiplet of levels in ^{27}Al resulting from weak coupling of a $1d^{5/2}$ proton hole to the 1.78-MeV 2^+ collective level in ^{28}Si . These are also the most strongly excited levels observed in 18-MeV ^3He scattering¹⁷ and 17.5-MeV proton scattering¹⁸ from ^{27}Al .

The inelastic scattering data are presented in Sec. V, where they are compared with DWBA calculations.

IV. OPTICAL MODEL ANALYSES

A. ^3He elastic scattering

A number of optical model fits to the ^3He elastic scattering angular distributions were performed, using the optical model codes GENOA¹⁹ and RAROMP,²⁰ with potentials of the Woods-Saxon form factor. Ambiguities in the real well depth V are known to exist,²¹ particularly at lower energies. There is also some ambiguity associated with the choice of surface or volume absorption.

In analyses of 59.8-MeV ^3He scattering from aluminum,⁹ the ambiguity in V was removed when large angle data were included; these analyses also indicated a preference for surface absorption over volume absorption. Artemov *et al.*²² analyzed 35.7-MeV ^3He elastic scattering data from a number of targets including ^{27}Al and ^{28}Si ; potentials

with $V \sim 160$ to 180 MeV gave equally good fits with either volume or surface absorption. In analyses of 37.7 -MeV ${}^3\text{He}$ scattering from ${}^{27}\text{Al}$ by Barnard and Jones²³ (with volume absorption only), potentials with $V \sim 110$ and 180 MeV gave similar (good) fits to the data.

Inasmuch as the present 46 -MeV data are at an energy intermediate between that of Refs. 22 and 23 and the 59.8 -MeV data of Ref. 9, we performed a grid-type analysis of the data from one of the targets— ${}^{29}\text{Si}$. A value was assigned to V and χ^2/N was minimized by varying the geometrical parameters for the real and imaginary wells. Then V was incremented and the procedure repeated. This sequence was followed at intervals of 10 MeV from $V = 80$ to $V = 220$ MeV. Subsequently, additional searches were performed at intermediate values of V near the extremities of discrete families of potential. For these searches a fixed value of $W_V = 20$ MeV was used and the spin orbit well depth was set at zero.

Plots shown in Fig. 2 summarize the results of the grid searches on the ${}^{29}\text{Si}$ data. Each of the plots in Fig. 2 (except the one for r_V) exhibits a pronounced systematic behavior characteristic of the discrete family ambiguity; the plot of r_R also shows the continuous $Vr_R^n \sim \text{const}$ ambiguity within each of the discrete families. The discrete family behavior of the diffuseness parameter is more pronounced than was observed in a similar analysis¹ of ${}^3\text{He}$ scattering from ${}^{60}\text{Ni}$. All of the potentials obtained from the grid searches (except for $V = 220$

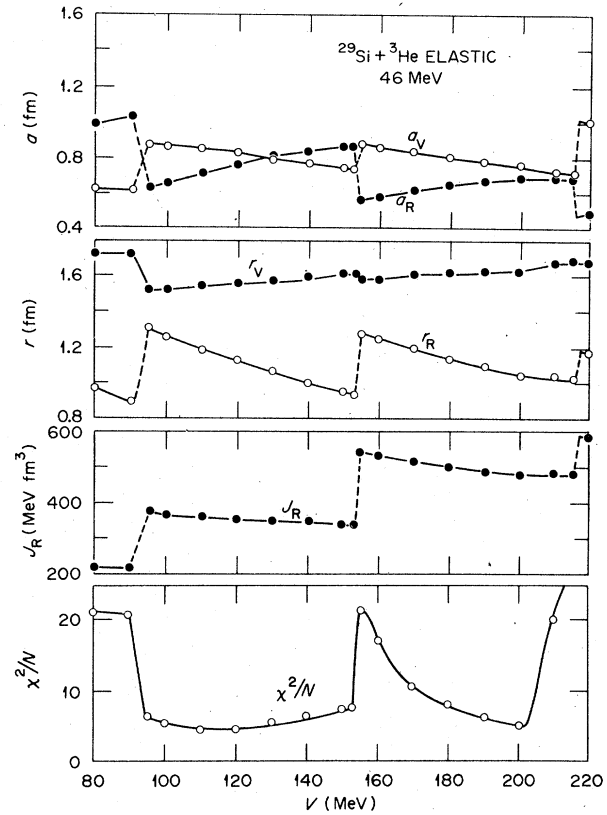


FIG. 2. Values of geometry parameters, volume integrals, and χ^2/N as functions of real well depth obtained from grid-type analysis of 46 -MeV ${}^3\text{He}$ elastic scattering data from ${}^{29}\text{Si}$. J_R is defined in the caption to Table I.

TABLE I. Parameters of the optical model potentials that yield the angular distributions compared with 46 -MeV ${}^3\text{He}$ scattering data in Fig. 1. Well depths are in MeV, geometry parameters are in fm, volume integrals are in MeV fm^3 . The value of r_R is 1.15 for all of the potentials. We define $J_R = (1/A_p A_t) 4\pi V \int r^2 f(r) dr$, where $f(r)$ is the radial form factor and A_p and A_t are, respectively, the projectile and target masses.

Target	Potential	V	a_R	W_V	r_V	a_V	W_D	r_D	a_D	J_R	χ^2/N
${}^{27}\text{Al}$	A	177.0	0.693				30.9	0.621	1.17	526	14.9
	B	176.8	0.693	41.2	1.10	1.12				525	16.3
	C	109.4	0.806				21.1	0.898	1.08	357	21.7
	D	110.3	0.803	23.9	1.47	0.928				359	19.4
${}^{28}\text{Si}$	A	182.3	0.695				29.3	0.964	0.947	538	10.5
	B	182.3	0.688	31.8	1.40	0.925				535	10.3
	C	117.9	0.804				23.4	1.21	0.797	381	14.4
	D	116.3	0.781	20.1	1.67	0.758				369	9.6
${}^{29}\text{Si}$	A	179.3	0.663				25.3	0.963	0.944	513	4.1
	B	179.4	0.653	25.6	1.45	0.888				509	4.4
	C	116.5	0.770				21.1	1.14	0.836	563	8.0
	D	116.0	0.753	19.1	1.60	0.807				357	5.8
${}^{30}\text{Si}$	A	177.9	0.653				26.0	0.810	1.07	502	9.8
	B	177.4	0.651	30.5	1.29	1.03				500	10.1
	C	114.1	0.748				20.6	0.991	0.989	347	12.9
	D	114.0	0.744	21.1	1.51	0.895				346	10.1

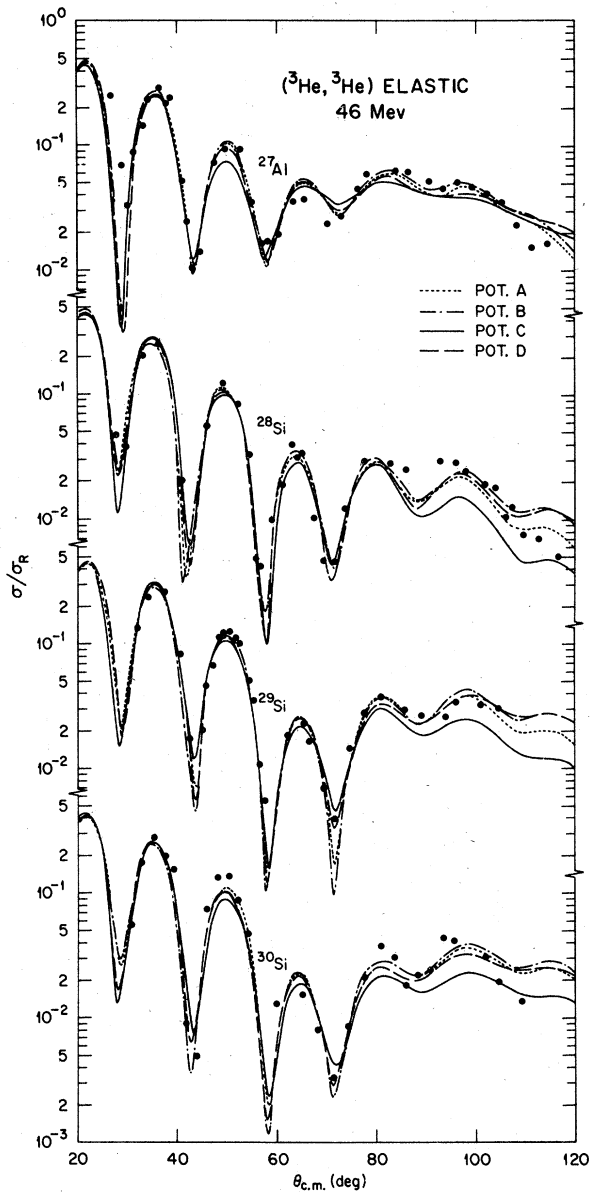


FIG. 3. Optical model fits to 46-MeV ^3He elastic scattering data. Parameters of the potentials are listed in Table I.

MeV) yield good fits to the data forward of $\sim 60^\circ$; the principal contribution to χ^2/N was from data at larger angles.

Six-parameter searches were performed for each of the four data sets with either volume or surface absorption and starting values of $V \sim 180$ and 120 MeV. Thus, for each target two fits were obtained for each of two discrete real well depth families. For these searches r_R was fixed at 1.15 fm (a value shown by grid searches on r_R to be

reasonable for all four targets) and a spin orbit well depth of zero was used. The parameter sets thus obtained are listed in Table I and Fig. 3 shows the fits to the experimental angular distributions. Only the ^{27}Al and ^{28}Si data sets contained any points at angles forward of the minima near 30° . These points, particularly for ^{27}Al , differed appreciably from all of the optical model predictions and were not used in calculating the χ^2/N values shown in Table I.

Generally, all four potentials obtained for each target give good overall agreement with the experimental angular distributions. In contrast to the results obtained for the 59.8-MeV data in Ref. 9, the analyses of the present 46 MeV data show no preference for either of the two discrete families of potential or for volume or surface absorption.

The ^3He data cover a smaller angular range than the α -particle elastic scattering data. The potentials that gave the best overall fit to the latter (discussed below) included both volume and surface absorption. A parameter search with both volume and surface absorption terms in the potential was tried for the ^{27}Al ^3He data with no improvement in the fit.

For the ^{27}Al data, a search with potential D of Table I with V_s (the spin-orbit well depth) as a variable parameter yielded a value of $V_s \sim 0.5$ MeV and a χ^2/N 5% smaller. Figure 4 compares the

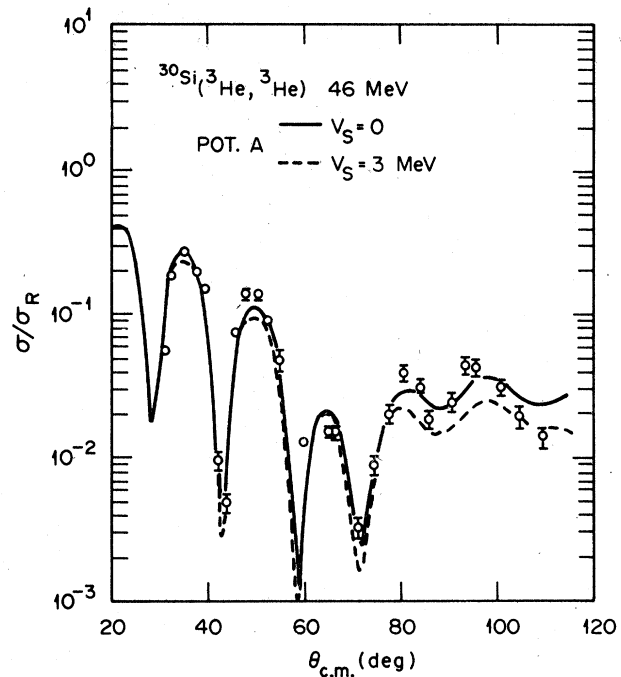


FIG. 4. Optical model predictions (with potential A of Table I) with $V_s = 0$ and 3 MeV compared with 46 MeV ^3He elastic scattering data from ^{30}Si .

^{30}Si data with angular distributions predicted (with potential A of Table I) with $V_s = 0$ and $V_s = 3$ MeV; for these calculations $r_s = r_R$ and $a_s = a_R$. As can be seen in Fig. 4, inclusion of the spin-orbit term has a negligible effect except at angles $>80^\circ$.

B. α -particle elastic scattering

A number of preliminary optical model analyses concentrated on the ^{28}Si data. Potentials of the Woods-Saxon form factor with either volume or surface absorption were obtained which would reproduce the general trend and gross features of the data but not the details of the structure in the angular distribution. Potentials with l -dependent volume absorption were also tried but with only moderate success. In contrast to ^{28}Si , data from the other isotopes, particularly ^{27}Al and ^{29}Si , were more easily fitted and a number of potentials with well depths corresponding to discrete families yielded good agreement with the data.

The best overall agreement with the data from all four targets was obtained in parameter searches for potentials that simultaneously include both volume and surface absorption with variable geometry parameters for each of the two absorption wells. The optical model parameters for two potentials thus obtained for each of the four targets are listed in Table II. Examples of these eight-parameter fits (r_R was fixed at 1.18 fm) to the data are shown in Fig. 5, where 40.1-MeV back angle data⁷ have been included.

The data shown in Fig. 5 span a large angular range. For ^{28}Si , 11 minima are observed in the angular distribution and nine or more are defined in the data shown for the other targets. The optical model fits are in rather good agreement with the data; almost all of the features of the data are reproduced, including the region between 80° and 150° where ^{28}Si data differ dramatically from that

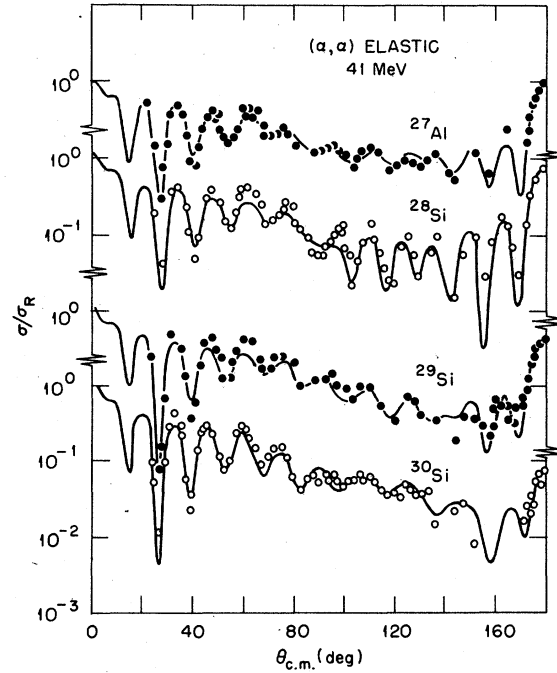


FIG. 5. Eight parameter fits to 41-MeV α -particle elastic scattering. Parameters of the potentials are listed in Table II. The data back of 160° are from Ref. 7. Parameters of the potentials are those of set A listed in Table II.

of the other targets. The back angle peaks, which exhibit a large variation in 180° cross section, are also fitted by the optical model potentials represented by the parameter sets listed in Table II.

The parameter sets in Table II show some interesting features. The values of a_V are surprisingly small and for ^{28}Si r_V is significantly smaller in the group A potentials than for the other targets. Increasing r_V for ^{28}Si to a value near that obtained for the other targets, as in the group B

TABLE II. Parameters of optical model potentials obtained from fitting the 41-MeV α -particle elastic scattering data presented in Fig. 1. Well depths are in MeV, geometry parameters are in fm, volume integrals are in MeV fm³. The value of r_R is 1.18 for all of the potentials. J_R is defined in the caption to Table I.

Target	Potential	V	a_R	W_V	r_V	a_V	W_D	r_D	a_D	J_R	χ^2/N
^{27}Al	A	179.1	0.736	27.2	1.38	0.23	4.88	1.53	0.590	440	8.5
	B	123.3	0.831	24.7	1.30	0.25	4.66	1.70	0.506	328	6.6
^{28}Si	A	177.4	0.740	43.8	0.995	0.195	6.32	1.60	0.446	434	20
	B	121.1	0.799	20.6	1.35	0.183	3.90	1.73	0.520	311	13
^{29}Si	A	172.1	0.710	30.2	1.38	0.232	5.95	1.31	0.745	408	16
	B	142.7	0.720	63.4	1.33	0.299	1.19	1.97	0.513	341	14
^{30}Si	A	167.0	0.769	25.6	1.34	0.145	8.47	1.62	0.458	412	18
	B	155.1	0.731	28.2	1.34	0.199	4.69	1.71	0.521	372	16

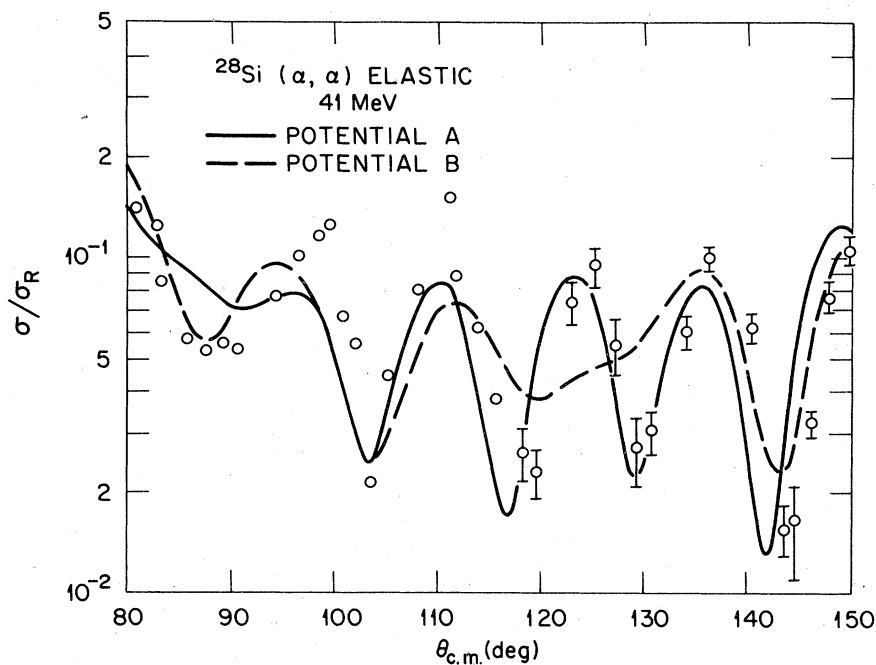


FIG. 6. Optical model predictions for 41-MeV α -particles on ^{28}Si compared with the data in the 80° - 150° region. Parameters of the potentials are listed in Table II.

potentials of Table II, resulted in a poorer fit, especially in the region between 80° and 150° , where the ^{28}Si data are most different from those of the other targets. This is demonstrated in Fig. 6.

A grid-type analysis, like that described above for ^3He scattering, was performed for the full angular range of the elastic α -particle data from ^{27}Al . Fixed values of $W_V = 25$ MeV and $W_D = 5$ MeV were used. For each value of V , χ^2 was minimized by varying the geometrical parameters of the real, volume absorption, and surface absorption wells. Results of this analysis, presented in Fig. 7, show some evidence for both the discrete families and the continuous Vr_R^n ambiguities in the optical model potentials that fit 41-MeV α -particle scattering over the almost complete angular range. Values of a_R were in the range of 0.7 to 0.8 fm; values of r_V were between 1.3 and 1.4 fm; and a_V values were between 0.2 and 0.3 fm. The values of r_W and a_W varied over the largest range; for $V < 120$ a_W was larger than r_W . The results presented in Fig. 7 suggest that potentials A and B of Table II for each target are in two discrete families, although the two values of V for ^{30}Si differ by only 12 MeV.

While good six-parameter fits were readily obtained for ^{27}Al and ^{29}Si data with small radius parameters and real well depths ~ 200 MeV in agreement with earlier studies,²⁴ the ^{28}Si and ^{30}Si angular distributions could be fitted well only by adding to the volume absorption a substantial surface ab-

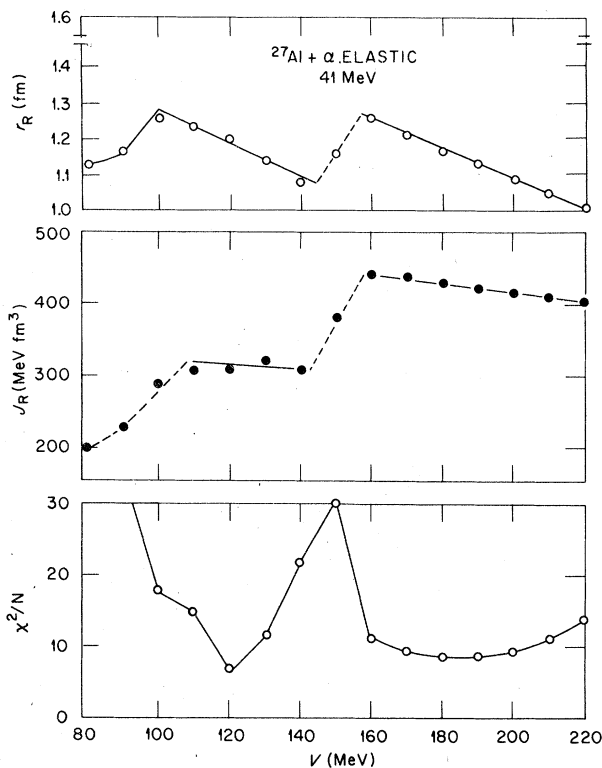


FIG. 7. Values of r_R , J_R , and χ^2/N as functions of real well depth for 41-MeV α -particle elastic scattering on ^{27}Al . The full range of the data shown in Fig. 1 was used in the grid-type analysis. J_R is defined in the caption to Table I.

sorption at large radius ($r_D \sim 1.60$ fm).

To emphasize the difference between the ^{28}Si α -particle data and these from the other targets, we show in Fig. 8 plots of the imaginary part of the complex wave number, $K_I(r)$, calculated with the parameters of group A potentials of Table II. The deep minimum at 3.5 fm in the ^{28}Si curve does not appear in a plot of $K_I(r)$ with parameters obtained from fitting the ^3He scattering data. It thus appears that the minimum observed in Fig. 8 for the best fit parameters obtained for the ^{28}Si α -particle data is evidence for some α -structure effect in the α -particle scattering. We also observe a shallower minimum at larger radius for the ^{30}Si plot in Fig. 8. Any parameter set we found that would reproduce the distinctive structure observed in the ^{28}Si data between 80° and 150° yielded a K_I vs radius plot like that shown in Fig. 8.

In the 22 MeV data of Ref. 12, the distinctive structure is not observed although there are differences between the ^{28}Si and ^{27}Al data. It thus appears that at this lower energy, α -particle elastic scattering is more limited to the nuclear surface and that the effect that produces the distinc-

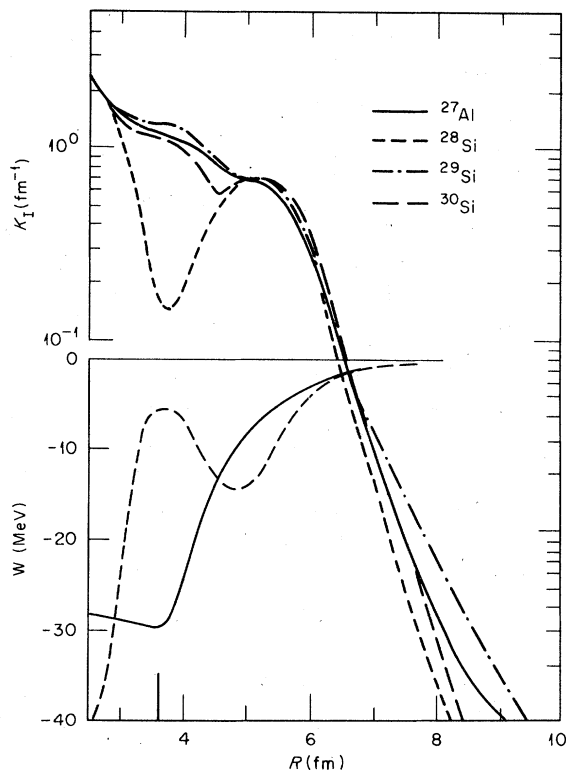


FIG. 8. Values of the attenuation coefficient K_I and imaginary potential $W = W_v + W_d$ as functions of R for 41-MeV α -particles. These were calculated for potential set A of Table II. The vertical line at 3.6 fm indicates the half-falloff radius of the real potential.

tive structure observed in the present ^{28}Si data has its origins in the nuclear interior.

The potentials characterized by the parameter sets listed in Table II were obtained in searches with eight variable parameters and one, r_R , common to all of the data sets. Further analyses were performed in which all four data sets were fitted simultaneously with additional parameters made common to all data sets while other parameters were data set dependent; only potential set A was used in this part of the analysis. The principal results of this were as follows: The diffuseness of the real well depth a_R could be set at 0.74 with only slight effect on the fits. If V was made common to all data sets, a value of $V = 176$ was obtained and the predicted cross sections for ^{30}Si near 180° are a factor of ~ 3 larger than the measured values. The region of ^{28}Si data between 80° and 150° was poorly fitted unless r_v was data set dependent and, for ^{28}Si , $\sim 25\%$ smaller than for the other targets.

V. ANALYSIS OF THE α -INELASTIC SCATTERING DATA

Distorted-wave Born-approximation calculations were performed, with the code DWUCK²⁵ for the α -particle inelastic scattering angular distributions measured in the present work. These calculations employed microscopic, collective form factors of the conventional potential-derivative form. The

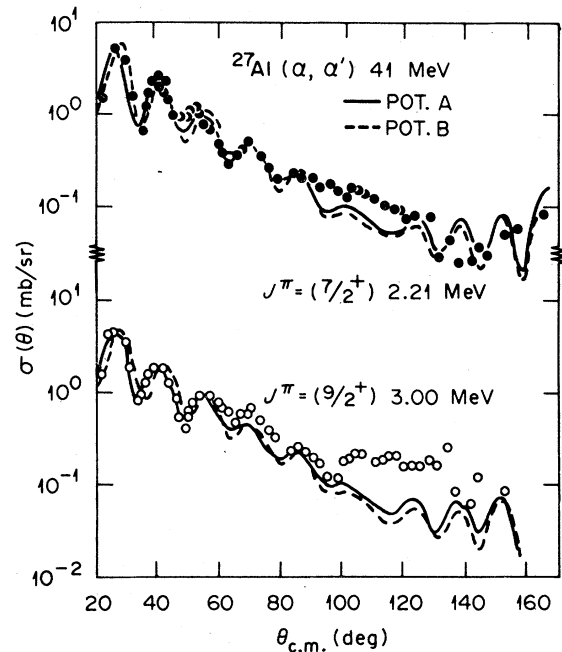


FIG. 9. Inelastic scattering angular distributions for 41-MeV α -particles on ^{27}Al compared with DWBA predictions for potentials A and B of Table II.

^{27}Al data are compared in Fig. 9 with the DWBA predictions obtained with both potentials A and B of Table II. For each of the levels, the calculated angular distributions are very similar for the two potentials, and good agreement with the data is obtained in the angular region forward of $\sim 100^\circ$.

Figure 10 compares the DWBA predictions, obtained with both sets of potentials, with the data from three silicon targets. Again the two calculated angular distributions are similar for both ^{29}Si and ^{30}Si . For ^{28}Si , however, the predicted angular distributions for the two potentials differ appreciably at angles larger than $\sim 80^\circ$, as was also observed above for elastic scattering. The fits to the data are reasonably good for both the $\frac{3}{2}^+$ level of ^{29}Si and the 2^+ level of ^{30}Si ; for the 2^+ level of ^{28}Si , good fits are obtained over a much smaller angular range.

Table III lists values of β_2 extracted from the DWBA fits and compares them with values reported from analysis of other scattering measurements. The values obtained in the present work for potentials A and B of Table II are in good agreement. The agreement with other work is reasonably good, especially for the silicon isotopes. We are aware of no published deformation parameters for ^{29}Si , although Coker *et al.*²⁷ have suggested a value of $\beta_2 = 0.35$ for the $\frac{3}{2}^+$ level based on an interpolation between β_2 values for ^{28}Si and ^{30}Si . The present results confirm this value.

Finally, since it was considered possible that the "anomalous" structure in the ^{28}Si α -particle elastic scattering could be due to coupling effects, coupled channels calculations were performed which included quadrupole and hexadecapole deformations. Even with parameter searching, fits to the elastic scattering data were not improved, although the fits to the inelastic scattering data were somewhat improved. It thus appears that the strongly oscillating structure, observed in the ^{28}Si α -particle elastic scattering data back of 80° , is

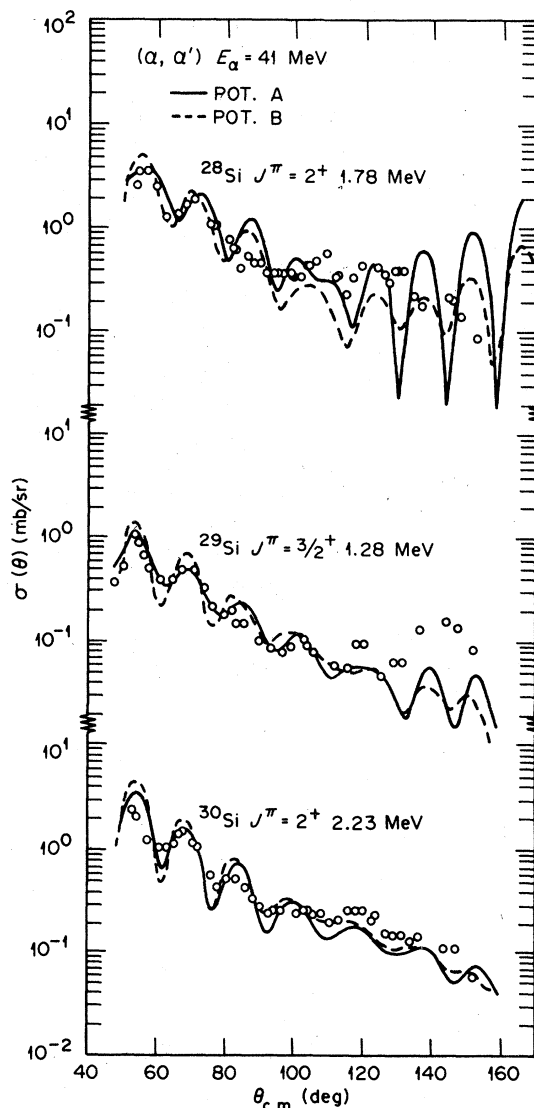


FIG. 10. Inelastic scattering angular distribution for 41-MeV α -particles on $^{28,29,30}\text{Si}$ compared with DWBA predictions for potential sets A and B of Table II.

TABLE III. Values of the quadrupole deformation parameter β_2 obtained from DWBA fits to inelastic scattering data. The parameters of potentials A and B are listed in Table II.

Nucleus	Level (MeV)	J^π	This work		Other work	β_2		Ref.
			Pot. A	Pot. B		Reaction	Reaction	
^{27}Al	2.21	$\frac{7}{2}^+$	0.41	0.39	0.56	$(^3\text{He}, ^3\text{He})$	18 MeV	17
					0.52	(p, p')	17.5 MeV	18
	3.0	$\frac{3}{2}^+$	0.36	0.34	0.36	$(^3\text{He}, ^3\text{He}')$	18 MeV	17
^{28}Si	1.78	2^+	0.43	0.41	0.48	(p, p')	17.5 MeV	18
					0.40	(p, p')	25 MeV	26
					0.32	(α, α')	104 MeV	27
^{29}Si	1.28	$\frac{3}{2}^+$	0.35	0.34	0.35	Interpolation		28
^{30}Si	2.23	2^+	0.38	0.40	0.31	(d, d')	11.8 MeV	29
					0.34	(α, α')	16 MeV	30

not principally due to effects of coupling to inelastic channels.

VI. SUMMARY AND CONCLUSIONS

We have presented measurements and analyses of scattering of 41 MeV α particles and 46-MeV ^3He for the same group of neighboring targets. The principal motivation was to examine the data for evidence of target spin effects such as were previously observed^{1,2} in both ^3He and α -particle elastic scattering from ^{59}Co and ^{60}Ni . A second motivation for the α -particle data is that they supplement the earlier back angle measurements⁷ to determine almost complete angular distributions.

For both particle types there is some qualitative evidence for target spin effects. This is limited to the angular region between $\sim 40^\circ$ and 70° , where minima observed in the ^{27}Al elastic angular distributions are shallower than the corresponding minima in the elastic angular distributions for the silicon targets. The evidence being limited to such a small range of angles, however, is less definitive than was observed earlier^{1,2} in a different target mass region.

A strong anomaly was observed in the α -particle elastic scattering from ^{28}Si which could be fitted well only by using optical model parameters different from those obtained by fitting data from

neighboring targets.

α -particle data for an almost complete angular range were fitted rather well with potentials that include both volume and surface absorption. A global optical model analysis failed to fit all four data sets by using parameters which vary smoothly with target mass; the most difficult regions were 80° – 150° for ^{28}Si and near 180° for ^{30}Si . Potentials with radial form factors different from the Woods-Saxon form factor were not explored in our analyses.

In the ^3He elastic scattering, the three silicon targets are very similar and different from ^{27}Al . It is possible that the difference is due to a target spin effect but unlikely due entirely to a quadrupole contribution. Good optical model fits to all of the ^3He angular distributions were obtained with either volume or surface absorption.

Grid-type searches show clearly both the discrete family and continuous Vr_R^n ambiguities in the 46-MeV ^3He elastic scattering and some evidence for the ambiguities in the α -particle scattering.

We conclude that α -particle scattering from ^{28}Si at 41 MeV exhibits an anomaly perhaps associated with an α -particle structure of this nucleus. More detailed measurements including excitation functions of elastic scattering are needed for a better understanding of the anomalous scattering.

*Operated by Union Carbide Corp. for the Department of Energy.

¹C. B. Fulmer and J. C. Hafele, *Phys. Rev. C* **7**, 631 (1973).

²C. B. Fulmer and J. C. Hafele, Electronuclear Div. Annu. Prog. Rep. 1970, Oak Ridge National Laboratory Report No. ORNL-4649, 1971 (unpublished) p. 47.

³G. H. Rawitscher, *Phys. Rev. C* **6**, 1212 (1972).

⁴N. M. Clarke, *J. Phys. A* **7**, 16 (1974).

⁵G. R. Satchler and C. B. Fulmer, *Phys. Lett.* **50B**, 309 (1974).

⁶See AIP Document No. PAPS PRVCA 18-621-15 for 15 pages of tabulated experimental elastic and inelastic cross sections. Order by PAPS number and journal reference from American Institute of Physics, Physics Auxiliary Publication Service, 335 East 45th Street, New York, N.Y. 10017. The price is \$1.50 for microfiche and \$5.00 for photocopies. Airmail additional. Make checks payable to the American Institute of Physics. This material also appears in *Current Physics Microfilm*, the monthly microfilm edition of the complete set of journals published by AIP, on the frames immediately following this journal article.

⁷C. B. Fulmer, D. C. Hensley, J. C. Hafele, C. C. Foster, N. M. O'Fallon, W. W. Eidson, and S. A. Grone-meyer, *Phys. Rev. C* **13**, 937 (1976);

⁷(a) C. B. Fulmer, D. C. Hensley, J. C. Hafele, C. C.

Foster, N. M. O'Fallon, W. W. Eidson, and S. A. Grone-meyer, *Phys. Rev. C* **13**, 937 (1976); (b) W. W. Eidson, C. C. Foster, C. B. Fulmer, S. A. Grone-meyer, D. C. Hensley, M. B. Lewis, N. M. O'Fallon, and R. G. Rasmussen, *Phys. Div. Annu. Prog. Rep.* 1973, Oak Ridge National Laboratory Report No. ORNL-4937 (1974), p. 65 (unpublished).

⁸J. W. Leutzelschwab and J. C. Hafele, *Phys. Rev.* **180**, 1023 (1969).

⁹C. B. Fulmer and J. C. Hafele, *Phys. Rev. C* **5**, 1969 (1972).

¹⁰P. Shapiro, L. S. August, J. J. Kolata, and L. R. Cooper, *Bull. Am. Phys. Soc.* **15**, 1679 (1970).

¹¹J. S. Blair and I. M. Naquib, *Phys. Rev. C* **1**, 569 (1970).

¹²J. Lega and P. C. Macq, *Nucl. Phys.* **A218**, 429 (1974).

¹³A. Bobrowska, A. Budzanowski, K. Grotowski, L. Jarczyk, S. Micek, H. Niewodniczanski, A. Strzalkowski, and Z. Wrobel, Institute of Nuclear Physics Report No. INP 624/PL, 1968 (unpublished).

¹⁴H. Oeschler, H. Schröter, H. Fuchs, L. Baum, G. Gaul, H. Lüdecke, R. Santo, and R. Stock, *Phys. Rev. Lett.* **28**, 11, 694 (1972).

¹⁵P. H. Stelson and L. Grodzins, *Nucl. Data* **A1**, 21 (1965).

¹⁶G. H. Fuller and W. V. Cohen, *Nucl. Data* **A5**, 433 (1969).

- ¹⁷J. E. Holden, D. P. Balamuth, H. T. Fortune, and R. W. Zurmüle, Phys. Rev. C 7, 611 (1973).
- ¹⁸G. M. Crawley and G. T. Garvey, Phys. Rev. 167, 1070 (1968).
- ¹⁹F. G. Perey and L. W. Owen (unpublished).
- ²⁰G. J. Pyle, Computer code RAROMP University of Minnesota Report No. COO 1265-64 (unpublished).
- ²¹C. M. Perey and F. G. Perey, At. Data Nucl. Data Tables 17, 1 (1976).
- ²²K. P. Artemov, V. Z. Goldberg, V. P. Rudakov, and I. N. Sezikov, Yad. Fiz. 13, 268 (1971) [Sov. J. Nucl. Phys. 13, 149 (1971)].
- ²³R. W. Barnard and G. D. Jones, Nucl. Phys. A108, 641 (1968).
- ²⁴K. W. Kemper, A. W. Obst, and R. L. White, Phys. Rev. C 6, 2090 (1972).
- ²⁵P. D. Kunz, University of Colorado Report No. COO-535-606 (unpublished).
- ²⁶R. de Swiniarski, H. E. Conzett, C. R. Lamontagne, B. Frois, and R. J. Slobodrian, Can. J. Phys. 51, 1293 (1973).
- ²⁷H. Rebel, G. W. Schweimer, G. Schatz, J. Specht, R. Löhken, G. Hauser, D. Habs, and H. Klewe-Nebenius, Nucl. Phys. A182, 145 (1972).
- ²⁸W. R. Coker, Takesh Udagawa, and G. W. Hoffmann, Phys. Rev. C 10, 1792 (1974).
- ²⁹W. Fitz, J. Heger, R. Santo, and S. Wenneis, Nucl. Phys. A143, 113 (1970).
- ³⁰W. Wühr, A. Hofmann, and G. Philipp, Z. Phys. 269, 365 (1974).